NUCLEAR THEORY, Vol. 41 (2024)
eds. M. Gaidarov, N. Minkov, Heron Press, Sofia

Microscopic Analysis of Elastic Scattering of One-Proton Halo Nucleus ^{17}F on Different Mass Targets

M.K. Gaidarov[1,2], **K.V. Lukyanov**[3], **E.V. Zemlyanaya**[3], **V.K. Lukyanov**[3], **D.N. Kadrev**[1], **A.N. Antonov**[1]

[1]Institute for Nuclear Research and Nuclear Energy, Bulgarian Academy of Sciences, 1784 Sofia, Bulgaria
[2]Department of Physics, Faculty of Mathematics and Natural Sciences, South-West University "Neofit Rilski", Blagoevgrad, Bulgaria
[3]Joint Institute for Nuclear Research, Dubna 141980, Russia

Abstract. An analysis of cross sections of elastic scattering of ^{17}F on ^{12}C, ^{14}N, ^{58}Ni, and ^{208}Pb nuclei at energy 170 MeV and on ^{208}Pb at various energies is carried out by using the microscopic optical potentials (OPs). The proton and neutron density distributions of the exotic nucleus ^{17}F are computed in the framework of microscopic models. The real part of the OP is calculated by a corresponding folding procedure accounting for the anti-symmetrization effects, while the imaginary part is obtained on the base of the high-energy approximation. In the hybrid model of the optical potential developed and explored in our previous works the only free parameters are the depths of the real and imaginary parts of the OPs obtained by fitting the experimental data. A good agreement of the theoretical results with the available experimental data is achieved pointing out clearly to a peripheral character of the scattering.

1 Introduction

Elastic scattering with stable nuclei provided most of the available information on the nuclear interaction potential, especially in the case of light projectiles, where both phenomenological and microscopic optical potential models have been developed to describe experimental results. With the secondary beams, these studies have gained renewed interest, since it became possible to measure elastic scattering for nuclei lying far from stability, to obtain the interaction potentials needed to analyze inelastic scattering or transfer reaction cross sections. Therefore, it is expected that reactions with these nuclei will provide a new direction for studying the exotic nuclear structures and new reaction mechanisms different from those of stable nuclei.

Most of the experiments with intensive secondary radioactive nuclear beams led to the discovery of halo nuclei on the neutron-rich side of the valley of stability [1, 2]. Although less probable, proton halos are also possible. Through

the last two decades, experimental data for the proton halo in proton-rich nuclei like ^{8}B have been reported in literature [3–5]. However, the amount of experimental data on the proton halo is relatively small compared to those on the neutron halo. In the present work the one-proton halo ^{17}F nucleus is in our focus. ^{17}F is a proton drip-line nucleus and it decays into ^{17}O+β^{+} with a half-life of 64.49 s. It has a low breakup threshold (0.6 MeV) into ^{16}O+p and its first excited state is a proton-halo state [6] which is bound by only 105 keV. The root-mean-square (rms) radius of the proton halo is 3.74 fm [6], significantly larger than that of the ^{16}O core (2.6 fm). The first excited state of ^{17}F (E_x=0.495 MeV and $J^{\pi} = 1/2^{+}$) has an extended rms radius of 5.3 fm, being the only bound state below the breakup threshold and is considered to be a proton halo state [6, 7]. The obtained value of the proton effective charge $e_p^{\text{eff}} = 1.12 \pm 0.07e$ extracted from the measured quadrupole moment is a strong evidence for the existence of a proton skin in the ground state of ^{17}F ($J^{\pi} = 5/2^{+}$) [8]. It can be anticipated that, given the exotic nature of ^{17}F, a lower reactivity than expected is generally observed.

In the present work (as well as in Ref. [9]), we analyze the data on elastic scattering cross sections of ^{17}F on ^{12}C [10], ^{14}N [10], ^{58}Ni [11], and ^{208}Pb [12] targets at energy 170 MeV and on ^{208}Pb [13, 14] at various energies within the microscopic hybrid model of OP and compare the results with the available experimental data using only two fitting parameters. They are related to the depths of the real (ReOP) and imaginary (ImOP) parts of the OP, where the latter is proportional to the effective cross section of the nucleon-nucleon (NN) interaction in nuclear matter. In addition, we test the nucleon density distribution of ^{17}F projectile which reflects its one-proton halo structure. The nuclear surface effects on the mechanism of the elastic scattering are also studied by looking at the ReOP and ImOP behavior in the periphery of the colliding nuclei in the case of ^{17}F+^{208}Pb reaction at a given energy.

2 The Microscopic Optical Potential

As in our previous works [15–21], where processes with neutron-rich He, Li, and Be isotopes and proton-rich ^{8}B nucleus were considered, we use the hybrid model of OP. The microscopic volume OP used in our calculations contains the real part (V^{DF}) including both the direct and exchange terms and the HEA microscopically calculated imaginary part (W^{H}). It has the form

$$U(r) = N_R V^{\text{DF}}(r) + iN_I W^{\text{H}}(r). \tag{1}$$

The parameters N_R and N_I entering Eq. (1) renormalize the strength of OP and are fitted by comparison with the experimental cross sections. Details of the constructing of the OP are given, e.g., in Refs. [22–25]. The real part V^{DF} consists of direct (V^{D}) and exchange (V^{EX}) double-folding integrals that include effective NN potentials and density distribution functions of colliding nuclei. The V^{D}

and $V^{\rm EX}$ parts of the ReOP have isoscalar (IS) and isovector (IV) contributions. The IS ones of both terms are

$$V^{\rm D}_{\rm IS}(r) = \int d^3r_p d^3r_t \rho_p(\mathbf{r}_p)\rho_t(\mathbf{r}_t) v^{D}_{\rm NN}(s), \tag{2}$$

$$V^{\rm EX}_{\rm IS}(r) = \int d^3r_p d^3r_t \rho_p(\mathbf{r}_p, \mathbf{r}_p+\mathbf{s})\rho_t(\mathbf{r}_t, \mathbf{r}_t-\mathbf{s}) v^{\rm EX}_{\rm NN}(s) \exp\left[\frac{i\mathbf{K}(r)\cdot s}{M}\right], \tag{3}$$

where $\mathbf{s} = \mathbf{r} + \mathbf{r}_t - \mathbf{r}_p$ is the vector between two nucleons, one of which belongs to the target and another one to the projectile nucleus. In Eq. (2) $\rho_p(\mathbf{r}_p)$ and $\rho_t(\mathbf{r}_t)$ are the densities of the projectile and the target, respectively, while in Eq. (3) $\rho_p(\mathbf{r}_p, \mathbf{r}_p + \mathbf{s})$ and $\rho_t(\mathbf{r}_t, \mathbf{r}_t - \mathbf{s})$ are the density matrices for the projectile and the target that are usually taken in an approximate form [26]. The expressions for the isovector direct and exchange components of the ReOP are given in Ref. [15]. The effective NN interactions $v^{\rm D}_{\rm NN}$ and $v^{\rm EX}_{\rm NN}$ have their IS and IV components in the form of M3Y interaction obtained within g-matrix calculations using the Paris NN potential [22]. The expressions for the energy and density dependence of the effective NN interaction are given, e.g., in Ref. [19].

It is important to note that the energy dependence of $V^{\rm EX}$ arises primarily from the contribution of the exponent in the integrand of Eq. (3). Indeed, there the local nucleus-nucleus momentum reads

$$K(r) = \left\{\frac{2Mm}{\hbar^2}\left[E - V^{\rm DF}(r) - V_c(r)\right]\right\}^{1/2} \tag{4}$$

with $M = A_pA_t/(A_p + A_t)$, where A_p, A_t, m are the projectile and target atomic numbers and the nucleon mass. As can be seen, $K(r)$ depends on the folding potential $V^{\rm DF}(r)$ that has to be calculated itself and, therefore, we have to deal with a typical non-linear problem.

Concerning the ImOP, we take it in the form that corresponds to the full microscopic OP derived in Refs. [27, 28] within the HEA [29, 30]:

$$W^{\rm H}(r) = -\frac{1}{2\pi^2}\frac{E}{k}\bar{\sigma}_{\rm N}\int_0^\infty j_0(qr)\rho_p(q)\rho_t(q)f_{\rm N}(q)q^2dq. \tag{5}$$

In Eq. (5) $\rho(q)$ are the corresponding form factors of the nuclear densities, $f_{\rm N}(q)$ is the amplitude of the NN scattering and $\bar{\sigma}_{\rm N}$ is the averaged over the isospin of the nucleus total NN scattering cross section that depends on the energy and accounts for the in-medium effects [31–33].

3 Results and Discussion

The OP [Eq. (1)] and the elastic scattering differential cross sections of ^{17}F on different targets are calculated using the DWUCK4 code [34] for solving the Schrödinger equation. All the elastic scattering cross sections will be shown in the figures as ratios to the Rutherford cross section.

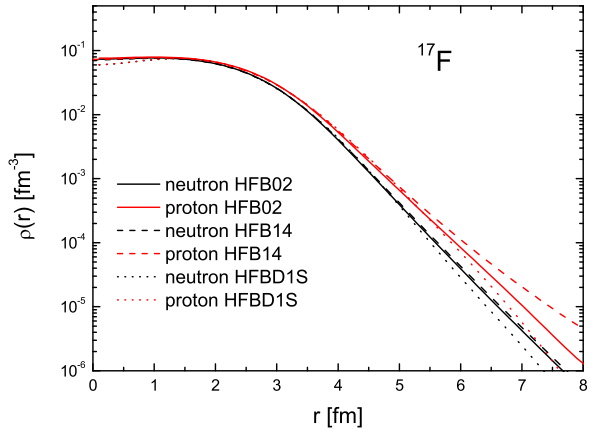

Figure 1. Proton and neutron density distributions of ^{17}Fe obtained in the HFB method [36] based on the BSk2 Skyrme [37] and D1S Gogny forces.

The real part of the OPs in the considered cases are calculated using Eqs. (1)-(4), while the imaginary part of the OPs is obtained using Eq. (5). Similarly to our previous works (for instance, Ref. [21]), we consider the set of the N_i coefficients [N_R and N_I; see Eq. (1) for the OP] as parameters to be found from the fit to the experimental data for the cross sections using the χ^2 procedure. The fitted N's related to the depths of the ReOP and ImOP can be considered as a measure of deviations of our microscopic OPs from the case when the values of N's are equal to unity.

Concerning the ^{17}F nucleus, we apply the neutron and proton density distributions [35] obtained within the Hartree-Fock Bogolubov (HFB) method [36] based on the BSk2 Skyrme force [37]. They are illustrated in Figure 1. The use of other effective Skyrme or Gogny forces in the HFB calculations does not change significantly the behavior of the densities, in particular of the proton ones in the surface region, where long tails are expected, typical for proton-rich halo nuclei. In the calculations of the OPs for ^{17}F+^{12}C the density of ^{12}C was taken in a symmetrized Fermi form with radius and diffuseness parameters 2.275 fm and 0.393 fm [38], respectively. For ^{17}F+^{58}Ni and ^{17}F+^{208}Pb elastic scattering the HFB densities of ^{58}Ni and ^{208}Pb [35] were used, while the density of ^{14}N calculated with the three-parameter Fermi model [39] was applied.

The calculated within the hybrid model elastic scattering cross sections of ^{17}F+^{12}C, ^{17}F+^{14}N, ^{17}F+^{58}Ni, and ^{17}F+^{208}Pb at energy $E = 170$ MeV in the laboratory frame are given in Figure 2 and compared with the experimental data [10–12]. In general, very good agreement with the available data is achieved for the elastic scattering processes on all different targets. It might be

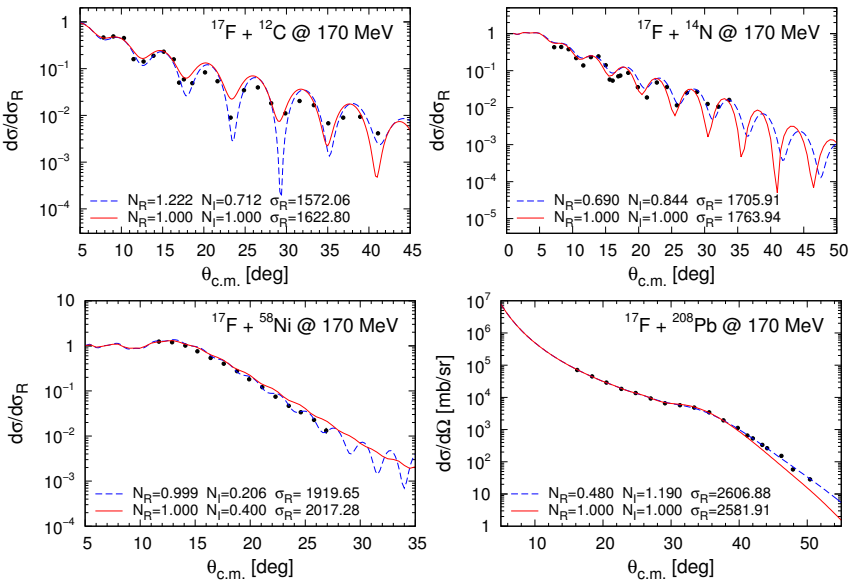

Figure 2. ^{17}F+^{12}C, ^{17}F+^{14}N, ^{17}F+^{58}Ni, and ^{17}F+^{208}Pb elastic-scattering cross sections at $E = 170$ MeV. Solid line: results without renormalization ($N_R = N_I = 1.000$) of both parts of OP (except for the case of ^{58}Ni target); dashed line: results with N_R and N_I which provide the best fit of the experimental data. The renormalization parameters N_R, N_I, and the total reaction cross sections σ_R (in mb) are given in the panels. Experimental data are taken from Refs. [10–12].

expected that an inclusion of inelastic and breakup channels in the calculation will not produce any substantial improvement at this energy. Our results reproduce the experimental data better than the analysis of the same data [40] with optical-model calculations using a double folding potential based on the density-dependent DDM3Y effective NN interaction for the real part of the OP, but the imaginary part of the optical potential has been taken in the phenomenological volume Woods-Saxon shape. Nevertheless, the obtained in Ref. [40] values for the reaction cross sections are in line with our values of σ_R. We observe that for all considered energies, σ_R increases with the increase of the energy E. Also, the reaction cross sections for the studied systems at 170 MeV increase with the increase of the target mass number A.

Further, we give in Figure 3 our results for ^{17}F+^{208}Pb elastic-scattering cross sections at energies 90.4 and 98 MeV near Coulomb barrier ($V_B = 91.7$ MeV as quoted in [41]). The information about the Coulomb barrier for a given process is useful to investigate the role of breakup (or other reaction mechanisms) for weakly bound exotic nuclei. The values of N_I deduced from the fitting procedure and shown in Figure 3 turn out to be substantially reduced to get better agreement with the experimental data. They are much smaller in comparison

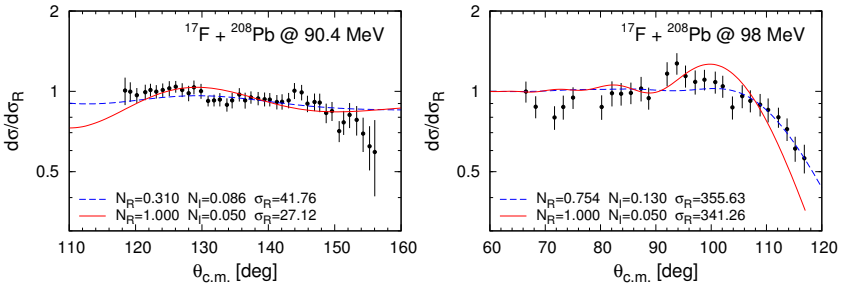

Figure 3. ^{17}F+^{208}Pb elastic-scattering cross sections at $E = 90.4$ MeV (below the Coulomb barrier) and $E = 98$ MeV (above the Coulomb barrier). The lines notation are the same as in Figure 2. The renormalization parameters N_R, N_I, and the total reaction cross sections σ_R (in mb) are given in the panels. Experimental data are taken from Ref. [13].

with the corresponding N_I values in the case of the same reaction at 170 MeV incident energy (see Figure 2). A similar observation was found in Ref. [20] from the analysis of the ^{8}B+^{58}Ni elastic scattering at near-Coulomb barrier energies. Also, both real and imaginary strong absorption radii were deduced from the optical model analyses of the same data [13]. The values of these radii reflect the surface interaction of the colliding nuclei. Obviously, more successful description of cross sections near Coulomb barrier can be achieved after inclusion of polarization contributions due to virtual excitations and decay channels of the reactions.

In order to estimate the role of the nuclear surface of the colliding nuclei on the mechanism of the elastic scattering, we focus on the shape of the ReOP and ImOP in their periphery. As an example, the renormalized depths of both parts of the calculated OPs used in the description of the ^{17}F+^{208}Pb elastic scattering data at $E = 170$ MeV are presented in Figure 4. The different curves correspond to different cases of parameters N_R and N_I that accept values in the interval between the two values shown in Figure 2, where one of them is unity (the non-normalized case). Moreover, all sets of optical potentials illustrated in Figure 4 lead to a good agreement with the experimental data. For instance, to get a better description of the 170 MeV data of ^{17}F+^{208}Pb elastic scattering within the microscopic CDCC model, a renormalization of the real part of the Koning-Delaroche potential by a factor 0.65 was required [42, 43] that is confirmed by the one of selected values N_R=0.645 in Figure 4. The behavior of all curves at distance $r \approx R(^{17}\text{F}) + R(^{208}\text{Pb})$, where R is the radius parameter of the two-parameter Fermi distribution, could serve as an indication for the reaction mechanism in the surface region around r. If one takes the values $R(^{19}\text{F})$=2.552 fm (the corresponding value of ^{17}F is missing and the closest isotope, for which R is available, is ^{19}F) and $R(^{208}\text{Pb})$=6.654 fm from Ref. [44], then their sum $r \approx 9.2$ fm. It is seen from Figure 4 that at this distance r the

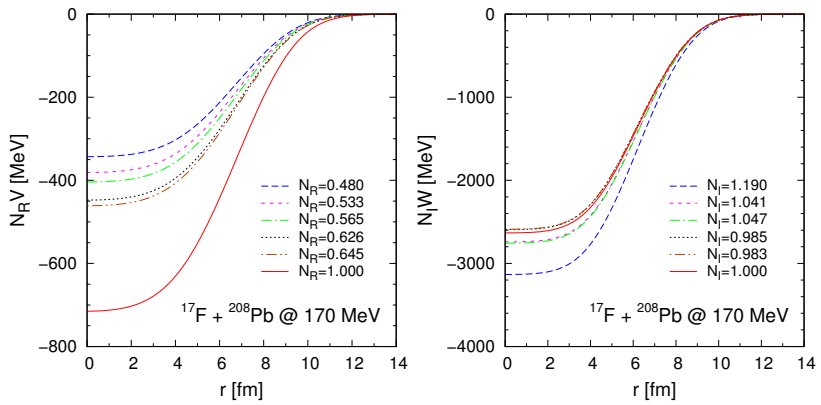

Figure 4. The renormalized depths $N_R V$ and $N_I W$ of the real and imaginary parts of OP [Eq. (1)] used in the calculations of the ^{17}F+^{208}Pb elastic-scattering cross sections at $E = 170$ MeV. The lines notations correspond to the different values of N_R and N_I including also the case $N_R = N_I = 1.000$.

real OP curves corresponding to different renormalization parameters N_R (except when N_R=1) are very close to each other exhibiting 30-40 MeV depth. The imaginary OP curves have a similar behavior with 160-180 MeV depth. This fact can be interpreted in a way that the whole scattering process is determined by the region of the far periphery [$r > R(^{17}\mathrm{F}) + R(^{208}\mathrm{Pb})$], where the potential curves practically coincide.

4 Summary and Conclusions

Microscopic calculations of the optical potentials and cross sections of elastic scattering ^{17}F+^{12}C, ^{17}F+^{14}N, and ^{17}F+^{58}Ni at 170 MeV, and ^{17}F+^{208}Pb at 90.4, 98, 120, and 170 MeV are performed, in comparison with the available experimental data. The direct and exchange isoscalar and isovector parts of the real OP (V^{DF}) were calculated microscopically using the double-folding procedure and density dependent M3Y (CDM3Y6-type) effective interaction based on the Paris NN potential. The imaginary part of the OP (W^{H}) was calculated microscopically as the folding OP that reproduces the phase of the scattering in the high-energy approximation. Microscopic densities of protons and neutrons in ^{17}F obtained in the framework of the HFB method [35] were used in the calculations. The free parameters of the model are the depths of the real and imaginary parts of the OP. Their values are obtained by fitting the experimental data on differential cross sections.

The main results from the work can be summarized as follows:

(i) Our calculations using microscopically derived optical model potentials reproduce successfully the measured angular distributions of elastic scattering

differential cross section and corresponding reaction cross sections at different energies above the Coulomb barrier.

(ii) We observe that for all considered energies for ^{17}F+^{208}Pb elastic scattering, the total reaction cross section σ_R increases with increasing the incident energy E. Also, the reaction cross sections for all considered systems at 170 MeV increase with increasing the target mass number A.

(iii) For the ^{17}F+^{208}Pb elastic scattering at 170 MeV at distances larger than 9 fm the real OP curves corresponding to different renormalization parameters N_R (except when N_R=1) are very close to each other exhibiting 30-40 MeV depth. The imaginary OP curves have similar behavior with 160-180 MeV depth. This is a clear indication of the role of the very far periphery, which is responsible for the behavior of the elastic scattering cross sections.

In general, we can conclude that our microscopic approach already applied to reaction studies with exotic nuclei such as ^{8}B [20] revealing a pronounced proton-halo structure can be successfully applied also to ^{17}F as an another one-proton halo nucleus.

References

[1] I. Tanihata, H. Hamagaki, O. Hashimoto, S. Nagamiya, Y. Shida, N. Yoshikawa, O. Yamakawa, K. Sugimoto, T. Kobayashi, D.E. Greiner, N. Takahashi, Y. Nojiri, *Phys. Lett. B* **160** (1985) 380.

[2] I. Tanihata, H. Hamagaki, O. Hashimoto, Y. Shida, N. Yoshikawa, K. Sugimoto, O. Yamakawa, T. Kobayashi, N. Takahashi, *Phys. Rev. Lett.* **55** (1985) 2676.

[3] A. Barioni *et al.*, *Phys. Rev. C* **84** (2011) 014603.

[4] E.F. Aguilera *et al.*, *Phys. Rev. C* **79** (2009) 021601(R).

[5] Y.Y. Yang *et al.*, *Phys. Rev. C* **87** (2013) 044613.

[6] R. Morlock *et al.*, *Phys. Rev. Lett.* **79** (1997) 3837.

[7] M.J. Borge *et al.*, *Phys. Lett. B* **217** (1993) 25.

[8] Zhou Dongmei *et al.*, *J. Phys. G* **34** (2007) 523.

[9] M.K. Gaidarov, K.V. Lukyanov, E.V. Zemlyanaya, V.K. Lukyanov, D.N. Kadrev, A.N. Antonov, *Phys. Part. Nucl.* **54** (2023) 500.

[10] J.C. Blackmon *et al.*, *Phys. Rev. C* **72** (2005) 034606.

[11] J.F. Liang *et al.*, *Phys. Lett. B* **681** (2009) 22.

[12] J.F. Liang *et al.*, *Phys. Rev. C* **65** (2002) 051603(R).

[13] M. Romoli *et al.*, *Phys. Rev. C* **69** (2004) 064614.

[14] J.F. Liang *et al.*, *Phys. Rev. C* **67** (2003) 044603.

[15] K.V. Lukyanov, V.K. Lukyanov, E.V. Zemlyanaya, A.N. Antonov, M.K. Gaidarov, *Eur. Phys. J. A* **33** (2007) 389.

[16] V.K. Lukyanov, E.V. Zemlyanaya, K.V. Lukyanov, D.N. Kadrev, A.N. Antonov, M.K. Gaidarov, S.E. Massen, *Phys. Rev. C* **80** (2009) 024609.

[17] V.K. Lukyanov, D.N. Kadrev, E.V. Zemlyanaya, A.N. Antonov, K.V. Lukyanov, M.K. Gaidarov, *Phys. Rev. C* **82** (2010) 024604.

[18] V.K. Lukyanov, E.V. Zemlyanaya, K.V. Lukyanov, D.N. Kadrev, A.N. Antonov, M.K. Gaidarov, K. Spasova, *Phys. Rev. C* **88** (2013) 034612; *Phys. At. Nucl.* **75** (2012) 1407.

[19] V.K. Lukyanov, D.N. Kadrev, E.V. Zemlyanaya, K. Spasova, K.V. Lukyanov, A.N. Antonov, M.K. Gaidarov, *Phys. Rev. C* **91** (2015) 034606.

[20] V.K. Lukyanov, D.N. Kadrev, E.V. Zemlyanaya, A.N. Antonov, K.V. Lukyanov, M.K. Gaidarov, K. Spasova, *Eur. Phys. J. A* **53** (2017) 31.

[21] V.K. Lukyanov, D.N. Kadrev, E.V. Zemlyanaya, K.V. Lukyanov, A. N. Antonov, M.K. Gaidarov, *Phys. Rev. C* **100** (2019) 034602.

[22] D.T. Khoa, G.R. Satchler, *Nucl. Phys. A* **668** (2000) 3.

[23] K.V. Lukyanov, JINR Comm. R11-2007-38, Dubna (2007).

[24] G.R. Satchler, W.G. Love, *Phys. Rep*. **55** (1979) 183; G.R. Satchler, "*Direct Nuclear Reactions*", Clarendon Press, Oxford (1983).

[25] M. Avrigeanu, G.S. Anagnostatos, A.N. Antonov, J. Giapitzakis, *Phys. Rev. C* **62** (2000) 017001; M. Avrigeanu, G.S. Anagnostatos, A.N. Antonov, V. Avrigeanu, *Int. J. Mod. Phys. E* **11** (2002) 249; M. Avrigeanu, A.N. Antonov, H. Lenske, I. Stetcu, *Nucl. Phys. A* **693** (2001) 616.

[26] J.W. Negele, D. Vautherin, *Phys. Rev. C* **5** (1972) 1472.

[27] K.V. Lukyanov, E.V. Zemlyanaya, V.K. Lukyanov, JINR Preprint P4-2004-115, Dubna (2004); *Phys. At. Nucl.* **69** (2006) 240.

[28] P. Shukla, *Phys. Rev. C* **67** (2003) 054607.

[29] R.J. Glauber, in *Lectures in Theoretical Physics* (New York, Interscience, 1959), p.315.

[30] A.G. Sitenko, *Ukr. Fiz. J.* **4** (1959) 152.

[31] S. Charagi, G. Gupta, *Phys. Rev. C* **41** (1990) 1610; **46** (1992) 1982.

[32] P. Shukla, arXiv:nucl-th/0112039.

[33] C. Xiangzhow, F. Jun, S. Wenqing, M. Yugang, W. Jiansong, Y. Wei, *Phys. Rev. C* **58** (1998) 572.

[34] P.D. Kunz, E. Rost, in *Computational Nuclear Physics*, edited by K. Langanke *et al.*, Springer-Verlag, New York (1993), Vol. 2, p. 88.

[35] Reference Input Parameter Library (RIPL-2): https://www-nds.iaea.org/RIPL-2/.

[36] M. Samyn, S. Goriely, P.-H. Heenen, J.M. Pearson, F. Tondeur, *Nucl. Phys. A* **700** (2002) 142.

[37] S. Goriely, M. Samyn, P.-H. Heenen, J.M. Pearson, F. Tondeur, *Phys. Rev. C* **66** (2002) 024326.

[38] V.V. Burov, D.N. Kadrev, V.K. Lukyanov, Yu.S. Pol', *Phys. At. Nucl.* **61** (1998) 525.

[39] H. De Vries *et al.*, *At. Data Nucl. Data Tabl.* **36** (1987) 495.

[40] Awad A. Ibraheem, Arwa S. Al-Hajjaji, M. El-Azab Farid, *Rev. Mex. Fis.* **65** (2019) 168.

[41] K.E. Rehm *et al.*, *Phys. Rev. Lett.* **81** (1998) 3341.

[42] J. Grineviciute, P. Descouvemont, *Phys. Rev. C* **90** (2014) 034616.

[43] J.J. Kolata, V. Guimarães, E.F. Aguilera, *Eur. Phys. J. A* **52** (2016) 123.

[44] J.D. Patterson, R.J. Peterson, *Nucl. Phys. A* **717** (2003) 235.